

# RSC Advances



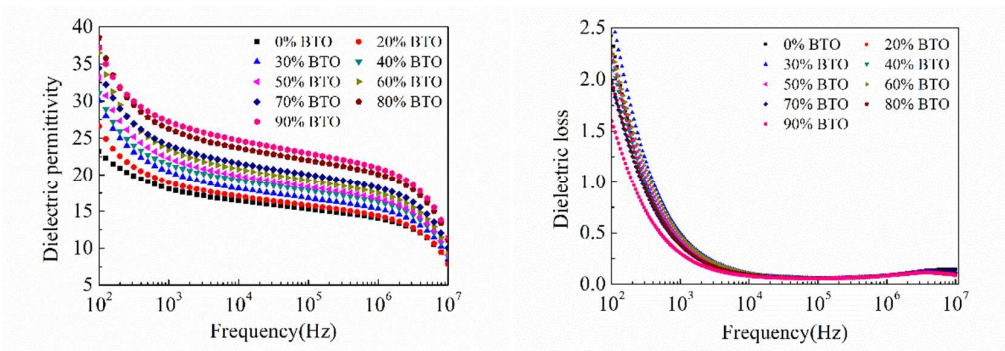
This is an *Accepted Manuscript*, which has been through the Royal Society of Chemistry peer review process and has been accepted for publication.

*Accepted Manuscripts* are published online shortly after acceptance, before technical editing, formatting and proof reading. Using this free service, authors can make their results available to the community, in citable form, before we publish the edited article. This *Accepted Manuscript* will be replaced by the edited, formatted and paginated article as soon as this is available.

You can find more information about *Accepted Manuscripts* in the [Information for Authors](#).

Please note that technical editing may introduce minor changes to the text and/or graphics, which may alter content. The journal's standard [Terms & Conditions](#) and the [Ethical guidelines](#) still apply. In no event shall the Royal Society of Chemistry be held responsible for any errors or omissions in this *Accepted Manuscript* or any consequences arising from the use of any information it contains.

## Table of Contents



Cyanoethyl cellulose-based high dielectric permittivity nanocomposite films were successfully prepared for the first time by introducing BaTiO<sub>3</sub> into cyanoethyl cellulose.

## ARTICLE

## Preparation and Dielectric Property of Cyanoethyl Cellulose/BaTiO<sub>3</sub> Flexible Nanocomposite Films

Cite this: DOI: 10.1039/x0xx00000x

Chao Jia, Ziqiang Shao,\* Haoyu Fan, Jianquan Wang

Received 00th January 2012,  
Accepted 00th January 2012

DOI: 10.1039/x0xx00000x

www.rsc.org/

Cyanoethyl cellulose(CEC)/BaTiO<sub>3</sub>(BTO) flexible nanocomposite films with enhanced dielectric property were successfully prepared by simple blend of CEC and BTO nanoparticles. The effects of BTO mass fraction on the morphology, microstructure, thermal stability, dynamic mechanical thermal analysis (DMTA), mechanical property, as well as dielectric property of the as-prepared nanocomposite films were investigated. The results showed that the BTO nanoparticles in size of about 100 nm were dispersed homogeneously in CEC matrix without obvious agglomeration. The obtained nanocomposite films possessed higher thermal stability than original CEC. DMTA revealed that the addition of BTO nanoparticles enhanced the glass transition temperature of the nanocomposite films. The mass fractions of BTO nanoparticles had a significant effect on the tensile strength and elongation at break of the nanocomposite films. The dielectric permittivity of the nanocomposite films decreased gradually with frequency, the dielectric loss decreased sharply at low frequency, and had little change at higher frequency. The dielectric permittivity of the nanocomposite films gradually increased with increasing mass fraction of BTO nanoparticles at all of the frequencies. The dielectric loss of the nanocomposite films had a tendency of decrease with increasing mass fraction of BTO nanoparticles at 10<sup>3</sup>Hz, but the dielectric loss almost remained unchanged at the higher frequency. When the mass fraction of BTO nanoparticles was 90%, the nanocomposite film had the biggest dielectric permittivity of 27.24 at 10<sup>3</sup>Hz, the corresponding dielectric loss was 0.3023.

### 1. Introduction

More and more attention has been paid to the high dielectric permittivity materials because they have a wide range of applications in the electrical and electronic industries<sup>1-3</sup>, such as high energy storage devices<sup>4-6</sup> and capacitors<sup>7-10</sup>. Ceramic-polymer nanocomposites for dielectric materials have attracted much interest due to their simple and convenient process, cheap cost, outstanding compatibility with printed wiring board (PWB) and excellent properties, such as lower dielectric loss, lower conductivity and leakage current<sup>11</sup>. Generally, polymers possess good processability and high breakdown strength, but their dielectric permittivity is relatively low. On the contrary, ceramics have high dielectric permittivity, but their processability is poor and breakdown strength is low<sup>12</sup>. Therefore, the incorporation of ceramics in the polymers is expected to be an effective method to develop high-performance nanocomposites with high dielectric permittivity. Up to now, many high dielectric permittivity ceramic filled polymer nanocomposites have been successfully fabricated<sup>5, 6, 13, 14</sup>.

Currently, the polymers used as matrices in the high dielectric permittivity nanocomposites mainly include poly(vinylidene fluoride) (PVDF) and its copolymers<sup>5, 15-19</sup>, polyimide<sup>12, 14, 20, 21</sup>, epoxy resin<sup>7, 11</sup>, polyethylene<sup>22</sup>, poly(methyl methacrylate)<sup>23</sup>, the

dielectric permittivities of all these polymers are less than 5 except PVDF and its copolymers. Compared with other ordinary polymers, PVDF and its copolymers possess higher dielectric permittivity, for example, P(VDF-CTFE) copolymer shows a dielectric permittivity of about 12 at 1kHz at room temperature and P(VDF-TrFE-CFE) terpolymer has a dielectric permittivity of around 55 at 1kHz at room temperature<sup>24</sup>. PVDF and its copolymers have been extensively studied in recent years<sup>24-27</sup>, and the composites using PVDF and its copolymers as the matrix, introducing a variety of ceramic fillers, have been fully researched as well<sup>28-35</sup>. Cyanoethyl cellulose(CEC) is a kind of cellulose ether, which can be prepared by Michael addition reaction of alkali-fied cellulose and acrylonitrile. It has some pretty unique properties, for example, resistant to microbial attack, good heat and acid stability, low moisture regain, good mechanical property. Cyanoethyl cellulose with high degree of substitution also has a high dielectric permittivity and low dielectric loss<sup>36</sup>, high water resistance, high insulation resistance and self-extinguishing performance. It can be applied in many fields, such as spinning, emulsifier, nonionic surfactant, electroluminescent material, it is the suitable candidate to be used to develop light converter of light-emitting diode(LED)<sup>37</sup>, large-screen television transmission screen, new radar screen and small laser capacitor for the optical weapons.

However, the potential of CEC as the matrix of high dielectric permittivity composites has not been fully explored. Therefore, it is necessary to use CEC as the polymer matrix, introduce common ceramic fillers into it, develop CEC-based high dielectric permittivity composites.

Barium titanate(BTO) nanoparticles are often employed as ceramic filler for polymer matrix composites because it is one of the most common commercially available high dielectric permittivity materials<sup>38</sup>. However, untreated BTO nanoparticles tend to form agglomerates<sup>6</sup>. It is well-known that the dielectric property of composite strongly relies on the dispersion of different components in the composite. Usually, the nanoparticles impart some special properties to the composite only when the nanoparticles are homogeneously dispersed in the polymer matrix<sup>13</sup>. Various strategies to prevent the aggregation of BTO nanoparticles embedded in the polymer matrix have been proposed, including surface hydroxylation<sup>6, 16</sup>, phosphonic acid modification<sup>39, 40</sup>, dopamine modification<sup>29, 41</sup>, modification with coupling agent<sup>18, 19</sup>, core-shell structure<sup>14</sup>.

As far as we know, the preparation of the composites by adding BTO nanoparticles to the CEC matrix has not been reported. In this work, CEC was chosen as polymer matrix and BTO nanoparticles (about 100 nm) was used as ceramic filler. The CEC/BTO nanocomposite films were prepared by using simple solution blending technique, the effects of BTO mass fraction on the morphology, microstructure, thermal stability, dynamic mechanical thermal analysis (DMTA), mechanical property, as well as dielectric property of the CEC/BTO nanocomposite films were investigated. The results will be helpful to realize the use of this kind of CEC-based nanocomposites with high dielectric permittivity in the embedded capacitor field.

## 2. Experimental

### 2.1. Materials

CEC was synthesized by using cotton as the raw material in our laboratory, the substitution degree of CEC was 2.57. BTO nanoparticles with average diameter of about 100 nm were purchased from Aladdin, and were used as received. Scanning electron microscope (SEM) images of the BTO nanoparticles are shown in Fig. 1. N, N-dimethylformamide(DMF) was used as the solvent to prepare the solution used to fabricate the CEC/BTO nanocomposite films by casting.

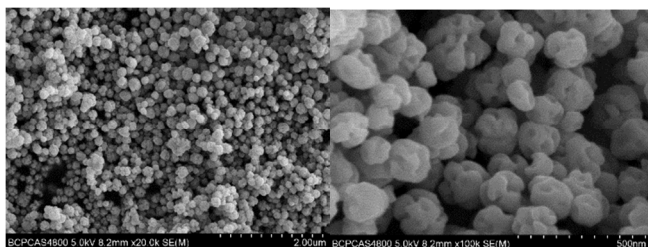


Fig. 1. SEM images of the BTO nanoparticles under different magnifications.

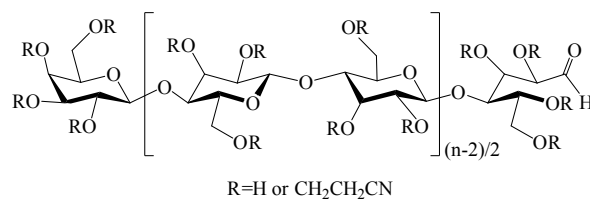
### 2.2. Preparation of CEC/BTO nanocomposite films

The CEC/BTO nanocomposite films were prepared by employing a simple solution blending technique. The BTO nanoparticles were ultrasonically dispersed in DMF for 1 h, at the same time, CEC powder was dissolved in DMF. Then the suspension of BTO was mixed together with the suspension of CEC. Afterwards, the mixture was magnetically stirred for 24h to obtain sticky and homogenous solution. Finally, the solution was cast on clean glass plates and dried at 60°C in an oven for 48h to ensure the complete evaporation of DMF. The prepared nanocomposite films loaded with various mass fractions of BTO nanoparticles and thickness of about 100µm were collected for test.

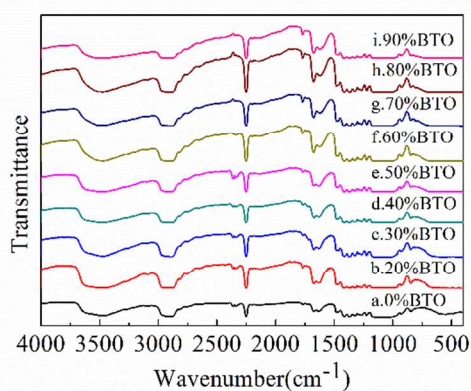
### 2.3. Characterization

The Fourier transform infrared spectroscopy (FTIR) spectra of CEC/BTO nanocomposite films were obtained by using a Fourier transform infrared spectrometer (Nicolet IS10) in transmission mode with a 2 cm<sup>-1</sup> resolution in the range of 4000–400 cm<sup>-1</sup>. The crystal phase structures of CEC/BTO nanocomposite films, as well as the BTO nanoparticles and CEC polymer, were determined by using a X-ray diffraction spectrometer(XRD, Rigaku) using Cu K<sub>α</sub> radiation in the 2θ range 5°–80°(40 kV, 40 mA). The morphology of the BTO nanoparticles and CEC/BTO nanocomposite films was characterized by field emission scanning electron microscopy(FESEM, HITACHI S-4800) with an accelerating voltage of 5kV. The mechanical property of CEC/BTO nanocomposite films was determined using a tensile tester (INSTRON 6022). Film specimens were cut into strips of 10mm×50 mm. Initial grip distance was set at 20 mm and the speed rate was 10 mm·min<sup>-1</sup>. The thermal stability of CEC/BTO nanocomposite films was performed on a heat heavy-difference heat integrated analyser(TG-DTA 6200 LAB SYS) from room temperature to 800°C in the nitrogen atmosphere, with a heating rate of 20°C/min. The dynamic mechanical thermal analysis (DMTA) of CEC/BTO nanocomposite films was performed on a intelligent rheometer(Physica MCR 301) with a solid DMTA test fixture at a frequency of 1Hz and the force was set to -1N. Film specimens were cut into strips of 10mm×50 mm. The range of temperature was from -100 to 200°C, the heating rate used was 5°C/min. The dielectric property of CEC/BTO nanocomposite films was measured using an impedance analyzer (Agilent 4294A) in the frequency range of 10<sup>2</sup> Hz to 10<sup>7</sup> Hz at ambient temperature. Prior to measurement, the nanocomposite films were cut into square samples of 0.9cm in width, the silver paste was painted on both sides of the samples to obtain the MIM structure for testing.

### 3. Results and discussion



(1)



(2)

Fig. 2. (1)Structural formula of CEC, (2)FTIR spectra of (a) pure CEC and (b-i)CEC/BTO nanocomposite films with different mass fractions of BTO nanoparticles.

Fig. 2 shows the structural formula of CEC and FTIR spectra of pure CEC and CEC/BTO nanocomposite films with different mass fractions of BTO nanoparticles. In the spectrum of pure CEC, there is a sharp band at  $2250\text{ cm}^{-1}$ , which is caused by the stretching vibration of nitrile groups ( $\text{C}\equiv\text{N}$ )<sup>42</sup>, there is a absorption band at  $995\sim 1168\text{ cm}^{-1}$ , which is assigned to the symmetrical and asymmetrical stretching vibrations of the ether groups ( $\text{C}-\text{O}-\text{C}$ ), both of them are the characteristics of CEC. There is a absorption band at  $3128\sim 3700\text{ cm}^{-1}$  (peak position at around  $3470\text{ cm}^{-1}$ ), which is resulted from the O-H stretching vibration<sup>42</sup>. In addition, a small signal observed at  $1672\text{ cm}^{-1}$  is assigned to the carbonyl groups as a result of the hydrolysis of acrylonitrile due to long reaction time in the preparation process of the CEC<sup>43</sup>. It can be seen that the introduction of BTO nanoparticles in the CEC matrix does not qualitatively alter the FTIR spectrum of CEC matrix.

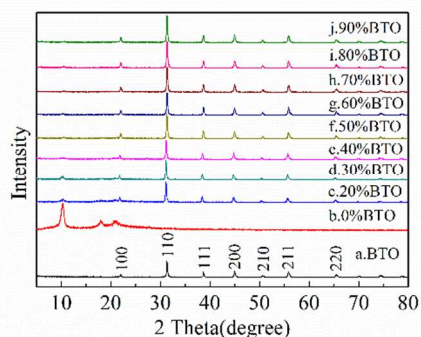


Fig. 3. XRD patterns of (a) BTO nanoparticles, (b) pure CEC and (c-j) CEC/BTO nanocomposite films with different mass fractions of BTO nanoparticles.

In order to study the stability of crystal phase structure of CEC and BTO in the process of nanocomposite films preparation, XRD patterns were obtained. Fig. 3 shows the XRD patterns of the original BTO nanoparticles, the pure CEC and the CEC/BTO nanocomposite films with different mass fractions of BTO

nanoparticles. The single crystal BTO nanoparticles have a pure perovskite phase<sup>13</sup>, and there is one characteristic peak at around  $45^\circ$ , which demonstrates that BTO nanoparticles we used have a cubic structure<sup>44</sup>. According to some reports, the size and structure of BTO nanoparticles have a significant influence on the dielectric property of the polymers<sup>11, 17, 44, 45</sup>. In comparison with the pure BTO nanoparticles, the XRD patterns of BTO nanoparticles in the nanocomposite films have no obvious changes. It indicates that the crystal phase structure of BTO nanoparticles is still stable when added them to the CEC matrix. However, the XRD patterns of CEC matrix in the nanocomposite films are different from that in pure CEC. CEC matrix has one diffraction peak at around  $2\theta\approx 10.3^\circ$ ,  $17.9^\circ$  and  $21.1^\circ$ , respectively. The peak intensity of CEC in the nanocomposite films decreases gradually with an increase of the BTO content. When the content of BTO increased to 50 wt%, the peak of CEC in the nanocomposite film disappeared completely. The decrease or even disappearance of the peak of CEC matrix could be due to the destruction of the ordered structure of the pure CEC matrix<sup>21</sup>. Maybe this is because the BTO nanoparticles dispersed in the CEC might have an important effect on the crystallization of the CEC matrix<sup>13</sup>. Therefore, the damage to the CEC crystallization becomes more and more obvious with the increasing mass fraction of BTO nanoparticles.

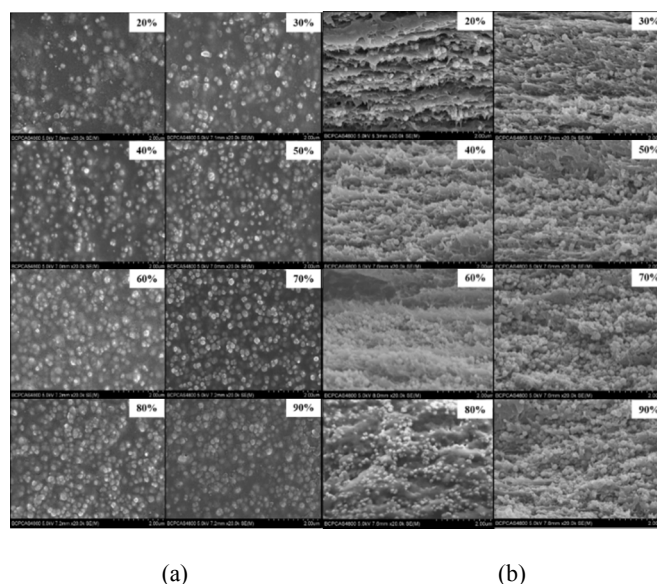


Fig. 4. SEM images of (a)top surfaces and (b)fractured cross sections of CEC/BTO nanocomposite films with different mass fractions of BTO nanoparticles.

The microscopic homogeneity of the CEC/BTO nanocomposite films was investigated by imaging the top surfaces and the fractured cross sections of nanocomposite films using a scanning electron microscope. Fig. 4 shows the SEM images of top surfaces and the fractured cross sections of CEC/BTO nanocomposite films with different mass fractions of BTO nanoparticles. It can be seen that BTO nanoparticles dispersed homogeneously in the CEC matrix. There is no obvious aggregation of BTO nanoparticles in the nanocomposite films, even if the mass fraction of BTO nanoparticles up to 90%. This result shows that uniform CEC/BTO nanocomposite films can be obtained by simple solution blending technique. The

size of BTO nanoparticles is still remained in near sphere shape with diameter of about 100 nm, the same to the original BTO nanoparticles. The packing of BTO nanoparticles becomes more and more dense with the increase of BTO content. All of these results indicate the excellent compatibility between the CEC matrix and the BTO nanoparticles.

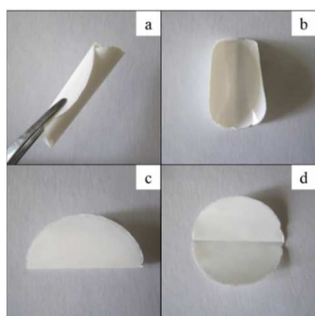


Fig. 5. Macroscopic photos of CEC/BTO nanocomposite film filled with 90 wt% of BTO nanoparticles to show its flexibility, (a) curly film, (b) unfolded film after being curled, (c) folded film, (d) unfolded film after being folded.

Fig. 5 shows the macroscopic photos of CEC/BTO nanocomposite film filled with 90 wt% of BTO nanoparticles in order to demonstrate its flexibility, a-d are the photos of curly film, unfolded film after being curled, folded film and unfolded film after being folded, respectively. From the photos it can be seen that the surface of the nanocomposite film is smooth, has no cracks and holes, and the film can be curled and folded, these results indicate that the nanocomposite film has excellent flexibility.

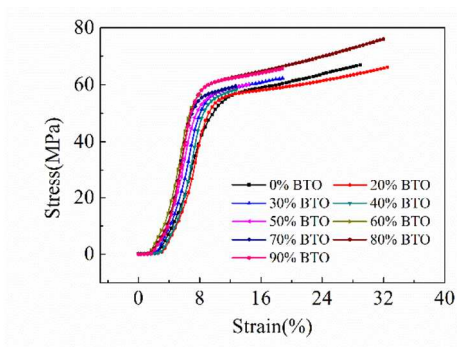


Fig. 6. Stress-strain curves of pure CEC and CEC/BTO nanocomposite films with different mass fractions of BTO nanoparticles.

The mechanical property of the neat CEC film as well as the nanocomposite films with different mass fractions of BTO nanoparticles was investigated by tensile testing at room temperature. The typical stress-strain curves of the neat CEC and CEC/BTO nanocomposite films are shown in Fig. 6. It could be seen that the nanocomposite films exhibit two characteristic regions of deformation behaviour. At low strain (<10%), the stress increases rapidly with increasing strain. The initial slopes are steep in the elastic region, indicating these films have relative high elastic moduli<sup>46</sup>. At higher strain, the stress gradually increases with an

increase of the strain up to the fracture of the nanocomposite films. There is no necking phenomenon in the stress-strain curves, which confirms the good dispersion of the BTO nanoparticles in the CEC matrix and homogeneous morphology of the nanocomposite films<sup>47</sup>, which is coincident with the result of their SEM images.

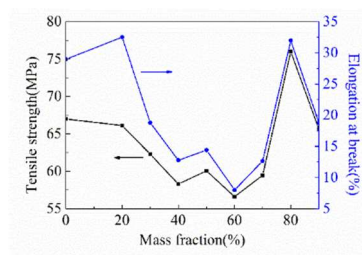


Fig. 7. The tensile strength and elongation at break of CEC/BTO nanocomposite films as a function of BTO nanoparticles content.

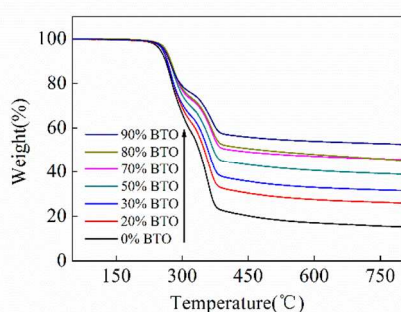
From the Fig. 7 we can see that the mass fraction of BTO nanoparticles has a profound effect on the tensile strength and elongation at break of the nanocomposite films, especially has significant impact on the elongation at break of the films. Pure CEC film has a tensile strength of 66.98MPa and elongation at break of 28.94%. It is interesting to note that the change trend of the elongation at break with increasing mass fraction of BTO nanoparticles is almost identical to the change of the tensile strength, which is different from the effect of reinforced material on the substrate material<sup>48, 49</sup>. At first, the tensile strength and elongation at break of the nanocomposite films display a decreasing trend with the increase of mass fraction of the BTO nanoparticles. When the mass fraction of BTO is 60%, the tensile strength and elongation at break have their minimum, are 56.62MPa and 8.00%, respectively. The decrease of the tensile strength and elongation at break can be attributed to the decrease of the crystallinity of the CEC matrix. Although the interaction between CEC matrix and BTO nanoparticles increases with increasing mass fraction of BTO nanoparticles, the contribution of the increasing interaction to the mechanical property of the nanocomposite films is less than the contribution of the decreasing crystallinity of the CEC matrix to the mechanical property. With the mass fraction of BTO continue to increase, the tensile strength and elongation at break begin to increase. Especially when the mass fraction of BTO is 80%, the tensile strength and elongation at break of the nanocomposite film increase dramatically to 75.99MPa and 31.98%, respectively, higher than the tensile strength and elongation at break of pure CEC film. The enhanced tensile strength and elongation at break may be due to the increased interaction between CEC matrix and BTO nanoparticles, which is in line with the TGA data.

The yield strength data of CEC and CEC/BTO nanocomposite films contain different mass fraction of BTO nanoparticles are listed in table 1. It can be seen that the mass fraction of BTO nanoparticles has relatively little effect on the yield strength of the nanocomposite films, especially when the mass fraction of BTO nanoparticles is less than 70%. When the mass fraction of BTO nanoparticles is higher than 70%, the yield strength of nanocomposite films increases, but the biggest yield strength of nanocomposite film only increases by 6% compared with that of CEC. We also can see from the data that

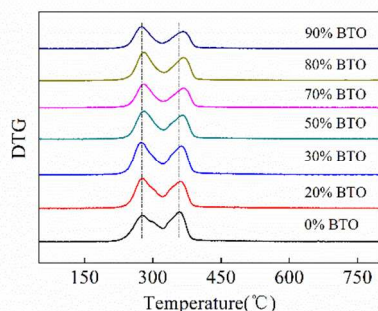
all the films have a yield strength of higher than 54 MPa, which indicates that CEC and CEC/BTO nanocomposite films have relatively high yield strength.

Table 1. Yield strength of CEC and CEC/BTO nanocomposite films contain different mass fraction of BTO nanoparticles.

Mass fraction of BTO nanoparticles(%)	Yield strength(MPa)
0	55.71
20	55.89
30	56.80
40	54.33
50	56.24
60	54.27
70	55.47
80	59.04
90	59.20



(a)



(b)

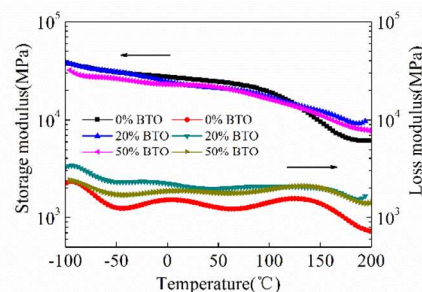
Fig. 8. (a)TG curves and (b)DTG curves of CEC and CEC/BTO nanocomposite films with different mass fractions of BTO nanoparticles.

The TG curves and DTG curves of CEC and CEC/BTO nanocomposite films with different mass fractions of BTO nanoparticles are shown in Fig. 8. The temperatures at 5.0% weight loss are 250.29, 256.05, 255.73, 261.22, 262.20, 263.03 and 259.45°C, respectively for the nanocomposite films containing 0, 20, 30, 50, 70, 80 and 90% of BTO nanoparticles by mass fraction. The doping of BTO nanoparticles improved the thermal stability of the nanocomposite films slightly. Table 2 lists the decomposition temperature of CEC and CEC/BTO nanocomposite films contain different mass fraction of BTO nanoparticles. It can be seen that the

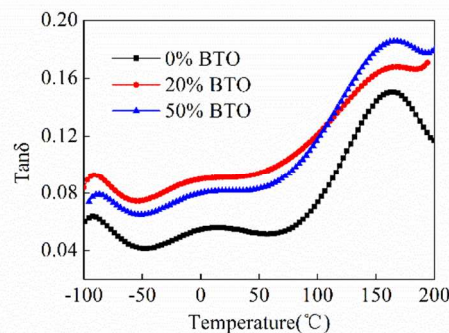
decomposition process of CEC includes two phases, the decomposition temperature of the first phase is 276.78°C, which may be resulted from the fracture of cyanoethyl groups, the decomposition temperature of the second phase is 358.47°C, which is caused by the damage of cellulose skeleton. We also can see that the decomposition temperature of the second phase increases steadily with the increase of the mass fractions of BTO nanoparticles until the mass fraction of BTO nanoparticles is 80%. When the mass fraction of BTO nanoparticles is 80%, the nanocomposite film has the highest decomposition temperature, which is 368.15°C, 9.68°C higher than the film without BTO nanoparticles. The increase of decomposition temperature can be attributed to the enhancement of interaction between the CEC matrix and the BTO nanoparticles, which limits the segmental movement of CEC<sup>12</sup>.

Table 2. Decomposition temperature of CEC and CEC/BTO nanocomposite films contain different mass fraction of BTO nanoparticles.

Mass fractions of BTO nanoparticles(%)	Decomposition temperature of the first phase (°C)	Decomposition temperature of the second phase (°C)
0	276.78	358.47
20	279.10	359.53
30	275.68	362.70
50	281.29	365.45
70	280.79	367.75
80	280.75	368.15
90	274.95	367.46



(a)



(b)

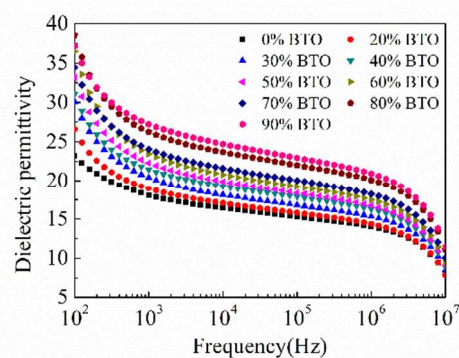
Fig. 9. (a)DMTA(storage modulus and loss modulus) and (b)DMTA(loss factor) of CEC and CEC/BTO nanocomposite films with different mass fractions of BTO nanoparticles.

DMTA is a very useful technique to study the viscoelastic response of the polymers as well as their composites in a wide range of temperature<sup>50</sup>. From the XRD patterns of CEC and CEC/BTO nanocomposite films we know that BTO nanoparticles have an important effect on the crystallization of the CEC matrix, and when the content of BTO nanoparticles increases to 50%, the crystallization of CEC in the nanocomposite film disappeared completely. Therefore, we want to know the influence of the increasing BTO content, namely the reducing crystallization of CEC on the viscoelastic response of nanocomposite films, so we obtained the DMTA data of CEC and CEC/BTO nanocomposite films with 20% and 50% BTO nanoparticles. Fig. 9(a) depicts the storage modulus and loss modulus of CEC and the nanocomposite films. It could be found that the storage modulus of the nanocomposite films shows a little decrease compared with that of the pure CEC film, and the loss modulus of the nanocomposite films increases. These results can be ascribed to the decrease of the crystallinity of the CEC due to the addition of BTO nanoparticles.

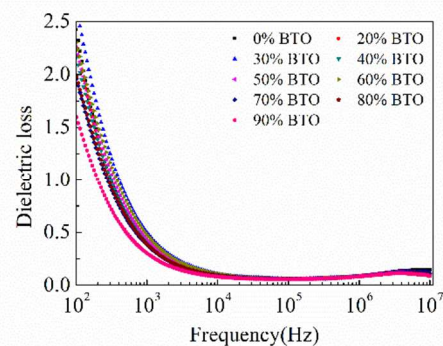
In general, the storage modulus decreases as the temperature increases. However, in the region corresponding to the maximum in the loss factor ( $\tan\delta$ ) curves, the decrease of storage modulus is generally rapid. Fig. 9(b) shows the curves of loss factor as a function of the temperature for CEC and CEC/BTO nanocomposite films. The loss factor is sensitive to the molecular motion and its peak is related to the transition temperature. It can be seen that all the curves reveal three thermal transitions, the transition temperatures are listed in table 3. The highest transition temperature is regarded as the glass transition temperature, which is caused by the motion of chain segments, the other two transition temperatures are secondary transition temperature, which can be attributed to the movement of side groups, end groups and other small constitutional units. From the table, we can see that the transition temperatures increase with the increasing mass fraction of BTO nanoparticles, enhanced transition temperature is associated with the interaction between CEC matrix and BTO nanoparticles.

Table 3. Transition temperatures of CEC and CEC/BTO nanocomposite films contain different mass fraction of BTO nanoparticles.

Mass fractions of BTO nanoparticles(%)	Glass transition temperature (°C)	$\beta$ transition temperature (°C)	$\gamma$ transition temperature (°C)
0	162.44	13.11	-92.67
20	167.27	18.79	-91.09
50	168.04	21.24	-86.61



(a)

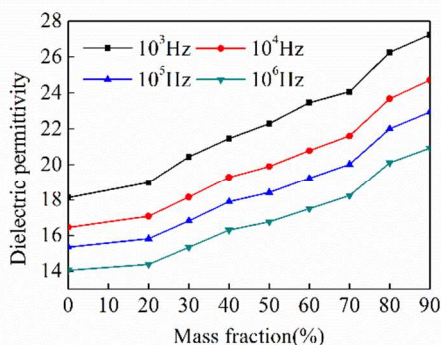


(b)

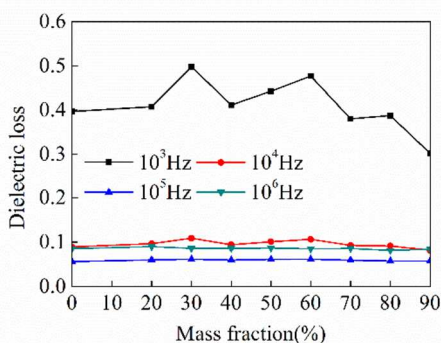
Fig. 10. Frequency dependence of (a)dielectric permittivity and (b)dielectric loss of pure CEC and CEC/BTO nanocomposite films with different mass fractions of BTO nanoparticles.

Fig. 10 presents the frequency dependence of dielectric permittivity and dielectric loss of pure CEC and CEC/BTO nanocomposite films with different mass fractions of BTO nanoparticles. It could be found that the dielectric permittivity of pure CEC and all nanocomposite films decreases gradually with frequency, especially in the range of  $10^2\sim 10^3$  Hz and  $10^6\sim 10^7$  Hz, at which the dielectric permittivity decreases sharply. However, there just has a small change within the scope of  $10^3\sim 10^6$  Hz. The dipole polarization of CEC matrix and BTO nanoparticles can be significantly enhanced at low frequency, these dipoles have enough relaxation time to catch up with the change of frequency, so that the dipole polarization make an important contribution to improve the dielectric permittivity of nanocomposite films at low frequency<sup>44</sup>. However, at high frequency, the dipoles do not have enough time to be polarized, thus the dielectric permittivity decreases as increasing frequency. For the dielectric loss of the nanocomposite films, we can see from the figure, it decreases sharply from  $10^2$  to  $10^4$  Hz, afterwards, it has little change as increasing frequency. Dielectric loss in a polymer-ceramic nanocomposite is related to the polarization mechanisms and the dipole relaxation associated with both materials, where the ceramic particles normally display lower dissipation at a given frequency<sup>6</sup>. As a result of the existence of polar cyanoethyl groups on the CEC matrix, so CEC has high

polarity, which leads to high intrinsic dipole moment. The dipole moments arrange directionally under the applied electric field, so orientation polarization occurs, which brings about the dielectric loss of CEC<sup>36</sup>. Compared with the CEC, BTO exhibits lower dielectric loss, and the dielectric loss of BTO reduces dramatically in the range of  $10^2$ – $10^3$  Hz<sup>51</sup>, which is coincident with the dielectric loss of CEC. Therefore, the significant decrease of the dielectric loss of the nanocomposite films could be the result of the interaction of CEC matrix and BTO nanoparticles.



(a)



(b)

Fig. 11. Dependence of (a) dielectric permittivity and (b) dielectric loss of the nanocomposite films on the mass fractions of BTO nanoparticles at different frequency.

The dependence of dielectric permittivity and dielectric loss of the nanocomposite films on the mass fractions of BTO nanoparticles at different frequency is presented in Fig. 11. It is observed that for the film without BTO nanoparticles, the dielectric permittivities are 18.12, 16.45, 15.34 and 14.04 at  $10^3$  Hz,  $10^4$  Hz,  $10^5$  Hz and  $10^6$  Hz, respectively. The dielectric permittivity of the nanocomposite films gradually increases with increasing mass fraction of BTO nanoparticles at all of the frequencies. When the mass fraction of BTO nanoparticles is 90%, the dielectric permittivities of nanocomposite film are 27.24, 24.71, 22.94 and 20.92 at  $10^3$  Hz,  $10^4$  Hz,  $10^5$  Hz and  $10^6$  Hz, respectively. The enhanced dielectric permittivity can be ascribed to the higher dielectric permittivity of BTO nanoparticles relative to CEC matrix<sup>5</sup> and the tight stacking of BTO nanoparticles in the nanocomposite films, the tight stacking of

BTO nanoparticles induces a strong interaction between BTO nanoparticles and CEC matrix<sup>38</sup>.

For the film without BTO nanoparticles, the dielectric losses are 0.3970, 0.0893, 0.0562 and 0.0854 at  $10^3$  Hz,  $10^4$  Hz,  $10^5$  Hz and  $10^6$  Hz, respectively. The dielectric loss of the nanocomposite films has a tendency of decrease with increasing mass fraction of BTO nanoparticles at  $10^3$  Hz, but the dielectric loss almost remains unchanged at the higher frequency. The decrease of dielectric loss with increasing mass fraction of BTO nanoparticles at  $10^3$  Hz is consistent with the dielectric loss result reported in the literature in which the dielectric loss of the nanocomposites decreases slightly with the BTO loading when the frequency is higher than  $10^2$  Hz<sup>23</sup>. The dielectric loss may mainly originate from the resonance of the CEC matrix at low frequency, hence reduction of the CEC content by increasing the mass fraction of BTO nanoparticles results in a decrease tendency of the dielectric loss of nanocomposite films<sup>6, 40</sup>. When the mass fraction of BTO nanoparticles is 90%, the dielectric losses of nanocomposite film are 0.3023, 0.0819, 0.0575 and 0.0840 at  $10^3$  Hz,  $10^4$  Hz,  $10^5$  Hz and  $10^6$  Hz, respectively. The dielectric loss of the nanocomposite films results primarily from the CEC matrix and is almost independent of the mass fraction of BTO nanoparticles, which indicates uniform dispersion of BTO nanoparticles in the nanocomposite films<sup>5</sup>.

As a caveat, the dielectric permittivity and dielectric loss of CEC we used are much higher than that reported in the reference 36, which may be due to the difference of substitution degree, the substitution degree of CEC we used is higher than that employed in the reference 36, the dielectric permittivity and dielectric loss of CEC enhance with increasing substitution degree according to the results obtained in this reference. In addition, according to the reference 36, the dielectric property of CEC is not only related to the substitution degree but to other parameters, such as the degree of order, the uniformity of distribution of the substituents and the bulkiness of the substituents.

#### 4. Conclusions

CEC/BTO flexible nanocomposite films could be successfully prepared by simple blend of CEC and BTO nanoparticles. The BTO nanoparticles in size of about 100 nm were dispersed homogeneously in CEC matrix without obvious agglomeration. The obtained nanocomposite films possessed higher thermal stability than original CEC. The addition of BTO nanoparticles enhanced the glass transition temperature of the nanocomposite films. The mass fraction of BTO nanoparticles has a significant effect on the tensile strength and elongation at break of the nanocomposite films. The dielectric permittivity of the nanocomposite films has good frequency stability within the scope of  $10^3$ – $10^6$  Hz, and the dielectric loss has good frequency stability in the range of  $10^4$ – $10^7$  Hz. The incorporation of BTO nanoparticles in the CEC matrix can significantly improve the dielectric permittivity of CEC, but has less impact on the dielectric loss. From what has been mentioned above, we can come to the conclusion that the obtained nanocomposite films should be a desirable candidate for high dielectric permittivity materials.

School of Material Science and Engineering, Beijing Institute of Technology, Beijing 100081, People's Republic of China

Beijing Engineering Technology Research Centre for Cellulose and Its Derivative Materials, Beijing 100081, People's Republic of China  
E-mail: jiachao0806@126.com; shaoziqiang@263.net

## References

- Z.-M. Dang, J.-K. Yuan, J.-W. Zha, T. Zhou, S.-T. Li and G.-H. Hu, *Prog Mater Sci*, 2012, **57**, 660-723.
- Z.-M. Dang, J.-K. Yuan, S.-H. Yao and R.-J. Liao, *Adv Mater*, 2013, **25**, 6334-6365.
- Q. Wang and L. Zhu, *J Polym Sci Pol Phys*, 2011, **49**, 1421-1429.
- H. M. Jung, J.-H. Kang, S. Y. Yang, J. C. Won and Y. S. Kim, *Chem Mater*, 2010, **22**, 450-456.
- J. Li, J. Claude, L. E. Norena-Franco, S. Il Seok and Q. Wang, *Chem Mater*, 2008, **20**, 6304-6306.
- M. N. Almadhoun, U. S. Bhansali and H. N. Alshareef, *Journal of Materials Chemistry*, 2012, **22**, 11196-11200.
- Z.-F. Zhang, X.-F. Bai, J.-W. Zha, W.-K. Li and Z.-M. Dang, *Compos Sci Technol*, 2014, **97**, 100-105.
- B. Balasubramanian, K. L. Kraemer, N. A. Reding, R. Skomski, S. Ducharme and D. J. Sellmyer, *Acs Nano*, 2010, **4**, 1893-1900.
- Y. Rao, S. Ogitani, P. Kohl and C. P. Wong, *Journal of Applied Polymer Science*, 2002, **83**, 1084-1090.
- Y. Wang, X. Zhou, Q. Chen, B. Chu and Q. Zhang, *Ieee T Dielect El In*, 2010, **17**, 1036-1042.
- Z.-M. Dang, Y.-F. Yu, H.-P. Xu and J. Bai, *Compos Sci Technol*, 2008, **68**, 171-177.
- S. H. Xie, B. K. Zhu, X. Z. Wei, Z. K. Xu and Y. Y. Xu, *Compos Part A-Appl S*, 2005, **36**, 1152-1157.
- Z. M. Dang, H. Y. Wang, Y. H. Zhang and J. Q. Qi, *Macromol Rapid Comm*, 2005, **26**, 1185-1189.
- Z.-M. Dang, Y.-Q. Lin, H.-P. Xu, C.-Y. Shi, S.-T. Li and J. Bai, *Adv Funct Mater*, 2008, **18**, 1509-1517.
- L. Xie, X. Huang, K. Yang, S. Li and P. Jiang, *Journal of Materials Chemistry A*, 2014, **2**, 5244-5251.
- T. Zhou, J.-W. Zha, R.-Y. Cui, B.-H. Fan, J.-K. Yuan and Z.-M. Dang, *ACS applied materials & interfaces*, 2011, **3**, 2184-2188.
- B.-H. Fan, J.-W. Zha, D. Wang, J. Zhao and Z.-M. Dang, *Appl Phys Lett*, 2012, **100**.
- X. Dou, X. Liu, Y. Zhang, H. Feng, J.-F. Chen and S. Du, *Appl Phys Lett*, 2009, **95**.
- Z.-M. Dang, H.-Y. Wang and H.-P. Xu, *Appl Phys Lett*, 2006, **89**.
- B.-H. Fan, J.-W. Zha, D.-R. Wang, J. Zhao and Z.-M. Dang, *Appl Phys Lett*, 2012, **100**.
- Z.-M. Dang, T. Zhou, S.-H. Yao, J.-K. Yuan, J.-W. Zha, H.-T. Song, J.-Y. Li, Q. Chen, W.-T. Yang and J. Bai, *Adv Mater*, 2009, **21**, 2077-2082.
- X. Y. Huang, P. K. Jiang and C. U. Kim, *J Appl Phys*, 2007, **102**.
- L. Xie, X. Huang, C. Wu and P. Jiang, *Journal of Materials Chemistry*, 2011, **21**, 5897-5906.
- B. Chu, B. Neese, M. Lin, S.-g. Lu and Q. M. Zhang, *Appl Phys Lett*, 2008, **93**.
- Z. Zhang and T. C. M. Chung, *Macromolecules*, 2007, **40**, 783-785.
- Z. Zhang, Q. Meng and T. C. M. Chung, *Polymer*, 2009, **50**, 707-715.
- W. Xia, Z. Xu, F. Wen, W. Li and Z. Zhang, *Appl Phys Lett*, 2010, **97**.
- S. Lin, X. Kuang, F. Wang and H. Zhu, *Phys Status Solidi-R*, 2012, **6**, 352-354.
- Y. Song, Y. Shen, H. Liu, Y. Lin, M. Li and C.-W. Nan, *Journal of Materials Chemistry*, 2012, **22**, 8063-8068.
- V. Tomer, E. Manias and C. A. Randall, *J Appl Phys*, 2011, **110**.
- W. Yang, S. Yu, R. Sun and R. Du, *Acta Mater*, 2011, **59**, 5593-5602.
- M. Arbatti, X. Shan and Z. Cheng, *Adv Mater*, 2007, **19**, 1369-+.
- X. Zhang, W. Chen, J. Wang, Y. Shen, L. Gu, Y. Lin and C.-W. Nan, *Nanoscale*, 2014, **6**, 6701-6709.
- P. Hu, Y. Shen, Y. Guan, X. Zhang, Y. Lin, Q. Zhang and C.-W. Nan, *Adv Funct Mater*, 2014, **24**, 3172-3178.
- J. Li, S. I. Seok, B. Chu, F. Dogan, Q. Zhang and Q. Wang, *Adv Mater*, 2009, **21**, 217-+.
- G. R. Saad, *Polym Int*, 1994, **34**, 411-415.
- H. Wang, Z. Shao, B. Chen, T. Zhang, F. Wang and H. Zhong, *Rsc Advances*, 2012, **2**, 2675-2677.
- Z.-M. Dang, D. Xie and C.-Y. Shi, *Appl Phys Lett*, 2007, **91**.
- P. Kim, S. C. Jones, P. J. Hotchkiss, J. N. Haddock, B. Kippelen, S. R. Marder and J. W. Perry, *Adv Mater*, 2007, **19**, 1001-+.
- P. Kim, N. M. Doss, J. P. Tillotson, P. J. Hotchkiss, M.-J. Pan, S. R. Marder, J. Li, J. P. Calame and J. W. Perry, *Acs Nano*, 2009, **3**, 2581-2592.
- Y. Song, Y. Shen, H. Liu, Y. Lin, M. Li and C.-W. Nan, *Journal of Materials Chemistry*, 2012, **22**, 16491-16498.
- W. Li, R. Liu, H. Kang, Y. Sun, F. Dong and Y. Huang, *Polymer Chemistry*, 2013, **4**, 2556-2563.
- X. Cao, S. Sun, X. Peng, L. Zhong and R. Sun, *Cellulose*, 2013, **20**, 291-301.
- Z.-M. Dang, H.-P. Xu and H.-Y. Wang, *Appl Phys Lett*, 2007, **90**.
- B.-H. Fan, J.-W. Zha, D.-R. Wang, J. Zhao, Z.-F. Zhang and Z.-M. Dang, *Compos Sci Technol*, 2013, **80**, 66-72.
- Y. Lu, L. Weng and X. Cao, *Carbohyd Polym*, 2006, **63**, 198-204.
- Y. C. X. Cao, P. R. Chang, A. D. Muir, G. Falk, *Express Polym Lett*, 2008, **2**, 502-510.
- L. Suryanegara, A. N. Nakagaito and H. Yano, *Compos Sci Technol*, 2009, **69**, 1187-1192.
- Y. Z. Wan, H. Luo, F. He, H. Liang, Y. Huang and X. L. Li, *Compos Sci Technol*, 2009, **69**, 1212-1217.
- X. Ma, P. R. Chang and J. Yu, *Carbohyd Polym*, 2008, **72**, 369-375.
- H. B. Sharma, H. N. K. Sarma and A. Mansingh, *J Appl Phys*, 1999, **85**, 341-346.